Effect of Postdrawing Temperature on Structure, Morphology, and Mechanical Properties of Melt-Spun Isotactic Polypropylene Tapes

Joachim Loos[*,†,‡,§] **and Tilo Schimanski**[†,⊥]

Laboratory of Polymer Technology, Laboratory of Materials and Interface Chemistry, Department of Chemical Engineering and Chemistry, and Dutch Polymer Institute, Eindhoven University of Technology, P.O. Box 513, 5600 MB Eindhoven, The Netherlands

Received June 10, 2005; Revised Manuscript Received September 25, 2005

ABSTRACT: Structure, morphology, and mechanical properties of melt-spun and postdrawn isotactic polypropylene (iPP) tapes are analyzed to study the effect of postdraw temperature applied. For affine drawing conditions, i.e., no effective relaxation of the molecules occurs during postdrawing, the Young's modulus is uniquely determined by the applied draw ratio. Only above a certain postdrawing temperature, the tensile modulus starts to decrease, indicating the onset of a nonaffine deformation, i.e., the occurrence of effective molecular relaxation during postdrawing. However, the overall mechanical behavior strongly depends on the postdrawing temperature used. For fixed draw ratios, a significant drop in yield stress can be observed with decreasing drawing temperature. Structural and morphological characterization indicates that, beside affine and nonaffine drawing regimes, mainly formation of the mesomorphic phase during solid-state drawing yields to the different mechanical behavior.

Introduction

The influence of various processing parameter and material characteristics on the mechanical properties of isotactic polypropylene (iPP) fibers or tapes has been reported extensively in the literature. It is commonly concluded that the tensile modulus depends uniquely on the applied draw ratio, as long as molecular relaxation can be avoided, i.e., for an affine deformation.[1,2] Moreover, it is emphasized in some studies that for an affine deformation the temperature in the drawing stage has no influence on the overall mechanical behavior of iPP.[1] However, in another study we have presented results which make the latter conclusion questionable.[3]

We have shown that the stiffness of samples depends only on the draw ratio used and is independent of the drawing temperature, which still is in accordance with the Irvine−Smith model for an affine deformation.[2] In contrast, yield stress and elongation at break are strongly influenced by the drawing temperature used. For a fixed draw ratio, a significant drop in yield stress can be observed with lowering the drawing temperature. This difference in mechanical behavior can be explained by drawing temperature-dependent variations of the samples crystal structures and morphologies. The main feature in this respect is the formation of the mesomorphic phase at low drawing temperatures.[4−10]

In the present study, the effect of postdrawing temperature on structure, morphology, and mechanical properties of melt-spun isotactic polypropylene tapes will be discussed. For this reason, solid-state postdrawn tapes were characterized using mechanical tensile tests, density, wide-angle X-ray, transmission electron microscopy, and shrinkage measurements to correlate thermal effects on mechanical properties with changes in structure and morphology.

Table 1. Weight-Average Molar Mass (M_w), Molar Mass Distribution (M_w/M_n), and Melt Flow Index (MFI; ISO 1133: T = 230 °C and m = 2.16 kg) of the iPP Materials Used in This Study

	M_w [kg/mol]	M_w/M_n	MFI [deg/min]
PLZ-937	500	5.6	1
X-7284	280	5.8	13
110E30SF	225	5.8	25

Experimental Section

Tapes have been produced from three different isotactic polypropylene materials, kindly supplied by Montell (PLZ-937; now Basell) and DSM (X-7284 and 110E30SF). The material characteristics are summarized in Table 1.

At Lankhorst/Indutech, The Netherlands, tapes were prepared on a melt spinning and solid-state drawing line consisting of extruder, nozzle, water bath (18 °C), godet, hot air oven with a length of ∼3 m, and winder. Godet and winder are rolls independent adjustable with different rotation speeds defining the input speed of the polymer fiber or tape in the oven and the output speed from the oven, respectively. For each material, the extruder conditions were optimized independently, but for a particular grade the extruder setup for all drawing experiments was identical. The postdraw ratio (λ_{PDR}) within the oven was determined by the ratio of the winder speed to the godet speed. For the samples studied, the godet speed was kept constant at 8 m/min. Different postdraw ratios were obtained by adjusting the velocity of the winder. All other processing parameters were kept constant. In the oven the tape was postdrawn at various temperatures ranging from 40 to 200 °C.

Additional heat treatment experiments have been performed on postdrawn tapes. For this, constrained as well as unconstrained tapes were annealed at 120 °C for 1 h. For the unconstrained samples, the decrease in length was calculated in percentage of the original length using the following equation:

$$x\,(\%) = \frac{l - l_0}{l_0} \times 100\% \qquad (1)$$

† Laboratory of Polymer Technology.
‡ Laboratory of Materials and Interface Chemistry, Department of Chemical Engineering and Chemistry.
§ Dutch Polymer Institute.
⊥ Current address: Intier Automotive, 80807 Munich, Germany. E-mail: Tilo.Schimanski@intier.com.
* Corresponding author. E-mail: j.loos@tue.nl.

10.1021/ma051223i CCC: $30.25
Published on Web 11/19/2005

l_0 and l are initial sample length and sample length after heat treatment, respectively.

Mechanical properties of the tapes were measured at room temperature with a tensile tester equipped with an extensometer, force reducing clamps, and a load cell of 500 N. The tensile tests were carried out with tapes of initial gauge length of 150 mm and at a crosshead speed of 150 mm/min. Force−elongation curves were recorded on a central section of the tapes with a length of 50 mm. A preload of about 0.5 N was applied on the samples. A set of 10 tensile tests was performed on each tape.

To relate the tensile force to the cross-section area, thickness and width of the tapes were measured. The thickness was determined with a twin-check layer thickness instrument using a magnetic-inductive method and a conventional mechanical thickness measurement device. Both instruments had a relative accuracy of about 1%. The width was measured with a magnifying glass equipped with a scale bar. For both dimensions, the average of 20 independent measurements, spread over a tape length of 20 m, was taken as the representative value.

The density of the tapes was measured at room temperature using a density gradient column. The column had a density gradient from 880 to 930 kg/m^3 and was prepared using distilled water and isopropyl alcohol according to the method described by Tung and Taylor.[11] The samples were allowed to seek their equilibrium position in the column for ~6 h. From the density measurements the mass crystallinity index X_c was calculated by using the following equation:[12,13]

$$X_c = \frac{\rho_c}{\rho}\left(\frac{\rho - \rho_a}{\rho_c - \rho_a}\right) \times 100\ (\%) \qquad (2)$$

ρ represents the measured density of the tape, $\rho_c = 938$ kg/m^3 is the density of the crystal phase, and $\rho_a = 854$ kg/m^3 is the density of amorphous isotactic polypropylene.

DSC measurements were performed on X-7284 tapes postdrawn to $\lambda = 5$ at 60 °C. A Perkin-Elmer DSC-7 differential scanning calorimeter was used, which was calibrated with zinc and indium as standards. The samples were held at 10 °C for 2 min and subsequently heated to 210 °C at a rate of 10 °C/min.

Wide-angle X-ray diffraction (WAXD) patterns were recorded on a transmission pinhole camera with an exposure time of 3 h. A Philips PW-1120 X-ray generator working at 40 kV and 30 mA produced the X-rays. The Cu Kα radiation had an average wavelength of 1.542 Å, while the Cu Kβ radiation was eliminated by a Ni filter. The 2D X-ray patterns were transformed into one dimensional plots by performing integration along the azimuthal angle. Afterward, the integrated plot was used to determine the position of the peak maximum of each reflection. At this particular angle, the azimuthal intensity distribution was measured in the 2D pattern. The full width half-maximum (fwhm) of the obtained intensity distribution pattern was calculated as a normalized measure for the arc length of the reflection.

For transmission electron microscopy (TEM) some tapes were stained with ruthenium tetraoxide (RuO_4).[14,15] Thin cross sections of these samples were prepared with a cryo ultramicrotom (Reichert Jung Ultracut E) and transferred on copper TEM grids. Investigation of the samples was performed using a JEOL 2000FX, operated at 80 kV in order to enhance contrast.

Results

Effect of Postdrawing Temperature on Mechanical Properties. In the present part of our study, the influence of postdrawing temperature on the overall mechanical behavior is illustrated. Figure 1 shows stress−strain curves of X-7284 tapes postdrawn to $\lambda_{PDR} = 5$ as obtained by tensile tests. The postdrawing temperature influences the overall mechanical properties of the tapes. This behavior is a general feature,

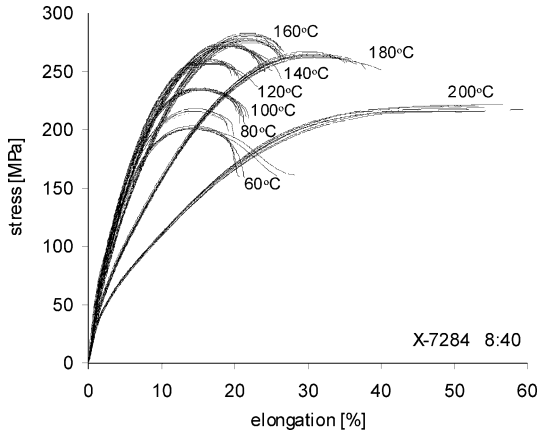

Figure 1. Stress−strain curves of (X-7284) tapes postdrawn to $\lambda_{PDR} = 5$ as obtained by tensile tests performed at room temperature. 8:40 reflects the ratio of godet speed (8 m/min) to winder speed (40 m/min). Drawing temperatures as indicated in the Figure.

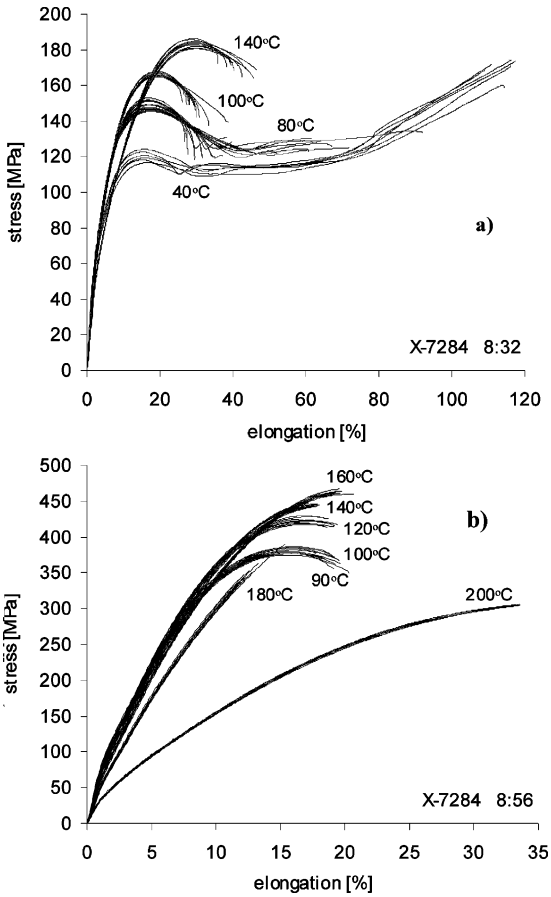

Figure 2. Stress−strain curves of (X-7284) tapes postdrawn to (a) $\lambda_{PDR} = 4$ and (b) $\lambda_{PDR} = 7$. The postdrawing temperatures are indicated in the figure.

which can also be observed for different postdraw ratios (Figure 2) and other iPP grades (Figure 3).

From the presented tensile test data, a significant influence of postdrawing temperature on the overall mechanical behavior can be seen. The tensile modulus of the postdrawn tapes remains constant up to a certain postdrawing temperature. Above this temperature, the stiffness of the tape decreases steeply with further increased postdrawing temperature. In Figure 4, the dependence of the tensile modulus on the postdrawing temperature is illustrated for X-7284 tapes with λ_{PDR}

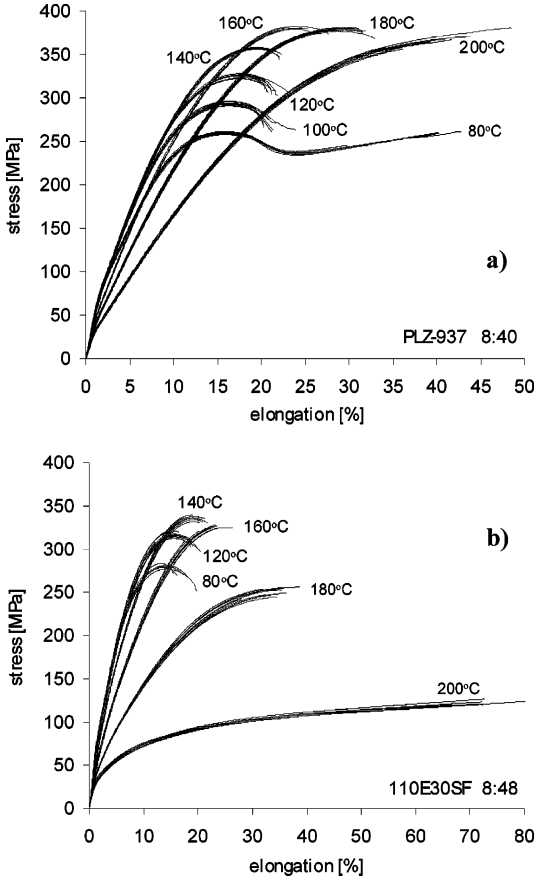

Figure 3. Stress−strain curves of (a) (PLZ-937)-tapes and (b) (110E30SF) tapes postdrawn to $\lambda_{PDR} = 5$ and $\lambda_{PDR} = 6$, respectively. The drawing temperatures are indicated in the figure.

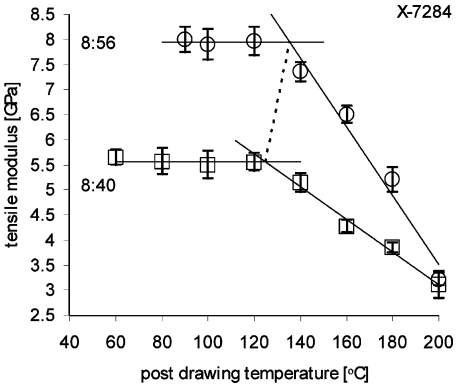

Figure 4. Tensile modulus as a function of the temperature applied in the postdrawing stage.

= 5 and $\lambda_{PDR} = 7$. The tensile modulus of the tape with $\lambda_{PDR} = 5$ remains constant at about 5.6 GPa up to postdrawing temperatures of about 120 °C. At higher temperatures, the tensile modulus decreases and reaches a value of about 3.1 GPa at a postdrawing temperature of 200 °C. At low postdrawing temperatures, the tapes with $\lambda_{PDR} = 7$ possess a plateau modulus of about 8 GPa, which also decreases at higher drawing temperatures, to about 3.2 GPa for the tape postdrawn at 200 °C.

From Figure 4, two different deformation regimes can be distinguished. The constant tensile modulus at low drawing temperatures indicates an affine deformation; i.e., no effective relaxation of the molecules occurs during postdrawing. Above a certain postdrawing temperature, the tensile modulus starts to decrease indicating the onset of a nonaffine deformation, i.e., the occurrence of effective molecular relaxation during postdrawing. The trend line sketched in Figure 4 may suggest a shift of the onset of the nonaffine deformation regime toward higher postdrawing temperatures with increasing postdraw ratio.

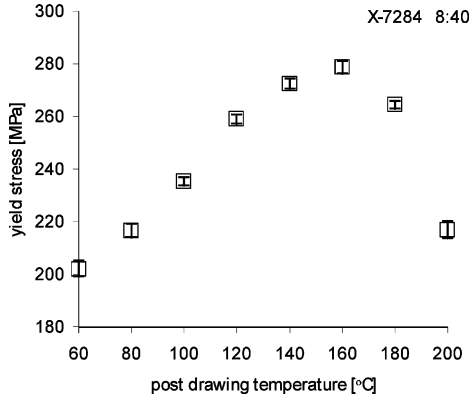

Figure 5. Yield stress in dependence on the temperature applied in the postdrawing stage.

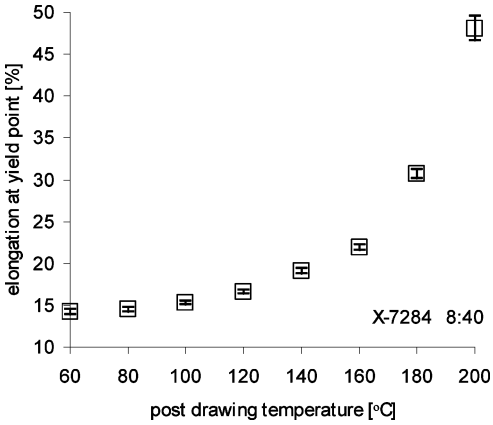

Figure 6. Elongation at yield point in dependence on the temperature applied in the postdrawing stage.

While the tensile modulus is independent of drawing temperature in the affine deformation regime, a strong dependence of the overall mechanical behavior can be found in both the affine and the nonaffine deformation regimes. Figure 5 shows the development of the yield stress as a function of postdrawing temperature for X-7284 tapes with $\lambda_{PDR} = 4$. The sketched error bars indicate the excellent reproducibility of the tensile measurements and, therefore, the remarkable homogeneity of the tapes.

Even in the affine deformation regime, the applied postdrawing temperature strongly affects the yield stress, increasing from about 200 MPa (for 60 °C) to about 260 MPa for the tape postdrawn at 120 °C. This behavior can be clearly seen, e.g., in the stress−strain curves of both the X-7284 tape with $\lambda_{PDR} = 4$ postdrawn at 40 °C (Figure 2a) and the PLZ-937 tape with $\lambda_{PDR} = 5$ (Figure 3a) postdrawn at 80 °C. The steady increase in yield stress continues in the nonaffine deformation regime to about 280 MPa for a postdrawing temperature of 160 °C, followed by a steep decrease to about 215 MPa for the tape postdrawn at 200 °C. Figure 6 shows the dependence of the elongation at the yield point on the postdrawing temperature. The small error bars again indicate the excellent reproducibility of the tensile test experiments. It can be seen that elongation at yield

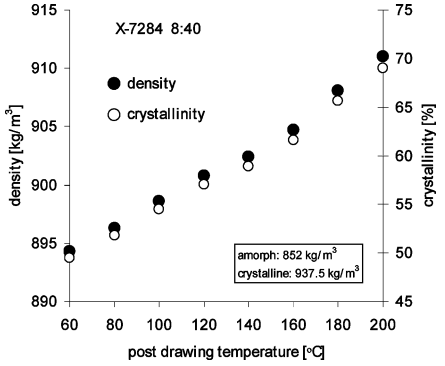

Figure 7. Density (and crystallinity) as a function of the postdrawing temperature for (X-7284) tapes with $\lambda_{PDR} = 5$.

point steadily increases with postdrawing temperature from about 15% at 60 °C to about 22% at 160 °C, followed by a steep increase to about 48% at 200 °C.

To examine whether the observed influence of postdrawing temperature on the overall mechanical behavior depends on sample geometry, additional tensile tests were performed on postdrawn iPP fibers. The mechanical behavior of the fibers is not as uniform as the behavior of the tapes; i.e., there is a larger spread in the stress−elongation curves. However, a similar dependence of the overall mechanical behavior on the postdrawing temperature used could be observed, which excludes restrictions on sample geometry (results not shown).

Influence of Postdrawing Temperature on Structure and Morphology. In this section, we describe the influence of postdrawing temperature used on structure and morphology of postdrawn tapes. The results are illustrated for X-7284 tapes with $\lambda_{PDR} = 5$. Figure 7 shows the influence of the postdrawing temperature used on the density of the tapes. The density increases almost linearly with increasing postdrawing temperature from about 894 kg/m^3 at 60 °C to about 911 kg/m^3 at 200 °C. Considering a two-phase model (crystalline and amorphous phase), the increase in density results from an increase in mass crystallinity with increasing postdrawing temperature. As indicated in Figure 7, the calculated mass crystallinity (open circles) increases from about 49.5% at 60 °C to about 69% at 200 °C postdrawing temperature. These are not absolute values since the density of the oriented (and constrained) amorphous phase in postdrawn tapes is expected to be higher than in the isotropic state; i.e., the values only illustrate a trend. Further, at low postdrawing temperatures, a mesomorphic phase may also exist, possessing an intermediate density. The mesomorphic phase may be induced by a partial transformation of crystalline and amorphous phases during postdrawing. The mesomorphic phase has a higher density ($\rho_{meso} \approx 880$ kg/m^3)[16] than the amorphous phase ($\rho_{amorph} = 854$ kg/m^3), but a lower density than the crystalline phase ($\rho_{cryst} = 938$ kg/m^3). The dependence of density on the postdrawing temperature used becomes more complex since the amount of the mesomorphic to alpha phase transformation depends again on the postdrawing temperature. Therefore, the main emphasis is on the increase in density with increasing postdrawing temperature, regardless of the mechanism involved.

Wide-angle X-ray scattering studies were performed to obtain information about the orientation of the crystal phase with respect to the drawing direction. Figure 8 shows diffraction patterns for various postdrawing

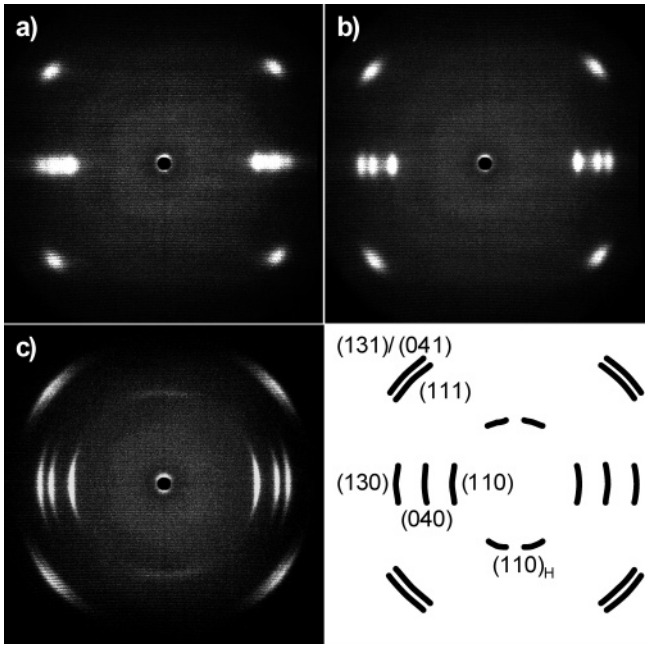

Figure 8. Wide-angle X-ray diffraction patterns of (X-7284) tapes postdrawn to $\lambda_{PDR} = 5$ at postdrawing temperatures of (a) 60, (b) 120, and (c) 200 °C.

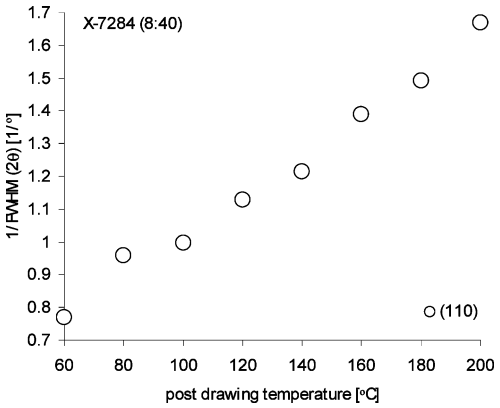

Figure 9. Inverse fwhm of the radial width of the (110) reflection as a function of the postdrawing temperature.

temperatures. Sharp reflections indicate a fiber pattern for all tapes. At low postdrawing temperatures the (110), (040), and (130) peaks as well as the (111) and (131)/(041) peaks are blurred. At higher drawing temperatures, the individual peaks are clearly distinguishable. This suggests a decreasing radial peak width with increasing postdrawing temperature. Since the radial peak width is inversely proportional to the size and/or perfection of the crystal, the fwhm of the radial width of the (110) reflection was determined. In Figure 9, the inverse of the determined fwhm value is shown as a function of the postdrawing temperature. The value increases steady with increasing postdrawing temperature. This indicates an increasing coherence of the crystals in the (110) direction with increasing postdrawing temperature, i.e., a lateral growth and/or perfection of the crystals. However, apart from the increase in lateral dimensions, the crystal size also increases along the *c*-direction with increasing postdrawing temperature. This can be seen from the transmission electron microscopy images presented in Figure 10. In the bright field TEM images brighter areas correspond to crystals surrounded by the dark because of the stained amorphous phase.

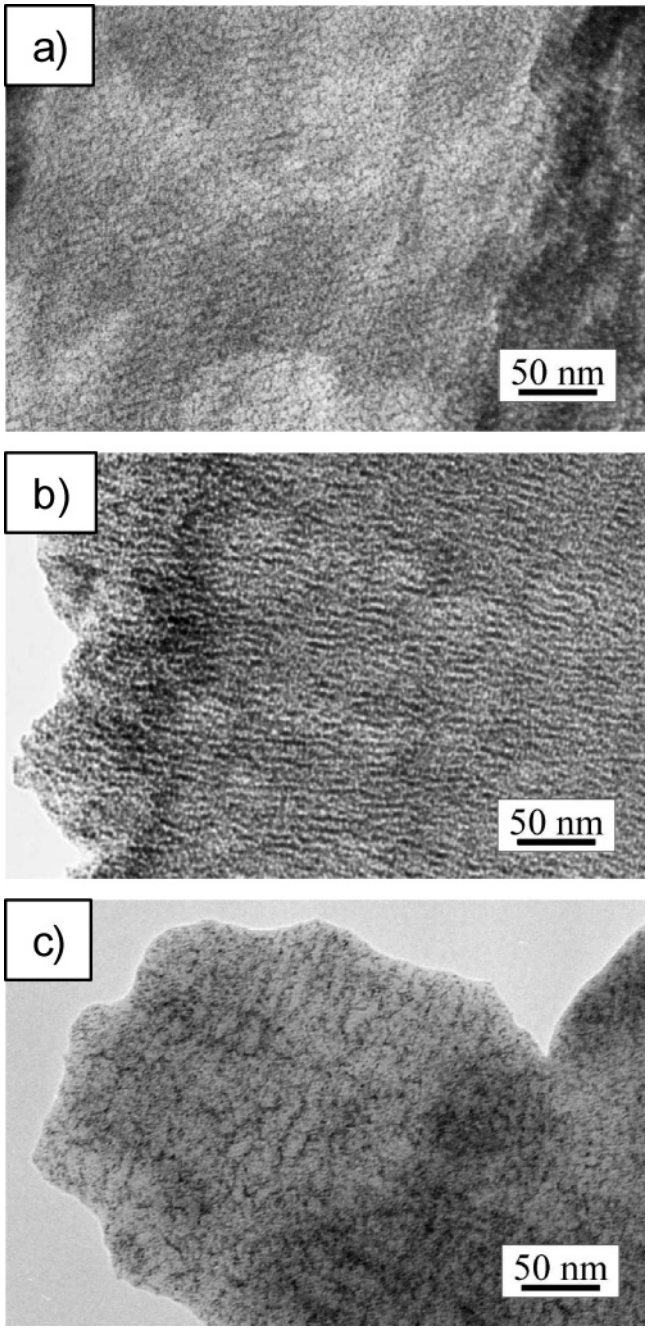

Figure 10. TEM images of the (X-7284) tapes postdrawn to $\lambda_{PDR} = 5$ at (a) 60, (b) 120, and (c) 200 °C.

The area shown in the TEM image of Figure 10a indicates that postdrawing at 60 °C results in formation of small crystal blocks. The size of the crystals increases with increasing postdrawing temperature; moreover, the parallel alignment of the crystals can be clearly observed for the tape drawn at 120 °C (Figure 10b). At a postdrawing temperature of 200 °C (Figure 10c), the crystals possess maximum size in both lateral and transversal directions. The alignment of the crystals is less ordered than at 120 °C.

From the X-ray diffraction patterns of Figure 8, it can be seen that the arc lengths of the diffraction peaks increase with increasing postdrawing temperature. The arc length reflects the breadth of the orientation distribution of the crystals, i.e., the fwhm of the arc length is inversely proportional to the average orientation of the crystals with respect to the drawing direction. The

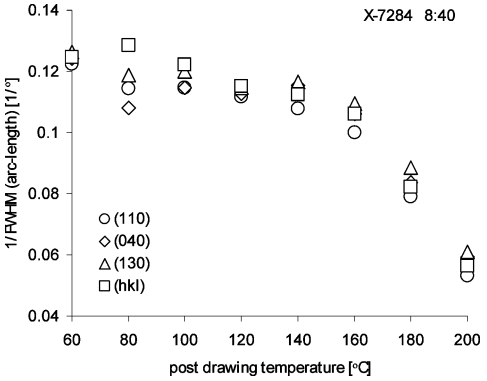

Figure 11. Inverse fwhm of the arc length of the indicated reflections in dependence on the applied postdrawing temperature.

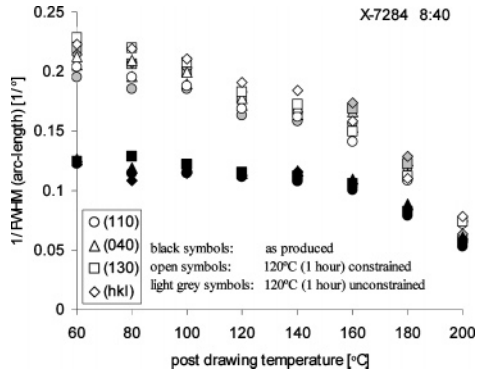

Figure 12. Inverse fwhm of the arc length of the indicated reflections in dependence to the initially applied postdrawing temperature.

inverse fwhm of the arc length was determined for the (110), (040), and (130) as well as the "(*hkl*)" reflections to quantify the average orientation of the crystal phase. The indices "*hkl*" summarize (111) and (131)/(041) reflections, which are blurred and not distinguishable at low postdrawing temperatures. The dependence of the fwhm values on the postdrawing temperature used is shown in Figure 11.

The inverse fwhm values, determined from the different reflections, are coherent with each other and follow the same trend. It can be seen that the average orientation of the crystals with respect to the drawing direction decreases slightly in the temperature range from 60 to 160 °C, followed by a steep decrease at higher postdrawing temperatures. At these temperatures (180 and 200 °C), additional $(110)_H$ reflections in the meridional direction appear in the diffraction pattern (Figure 8), indicating homoepitaxial crystal growth.

Additional wide-angle X-ray scattering studies have been performed on tapes annealed at 120 °C for 1 h. Figure 12 shows the inverse fwhm of the arc length for the (110), (040), and (130) as well as the "(*hkl*)" reflections. The heat treatment was carried out on constrained (open symbols) and unconstrained (light gray symbols) tapes. For comparison, the data obtained from the initial tape are included (black symbols).

Comparing the inverse arc length fwhm values of the initial tape with the data for the annealed samples, it can be seen that heat treatment improves the alignment of the crystals with respect to the drawing direction, especially for tapes postdrawn at low temperatures. Figure 13 illustrates the influence of the additional heat treatment on the radial width of the (110) reflection.

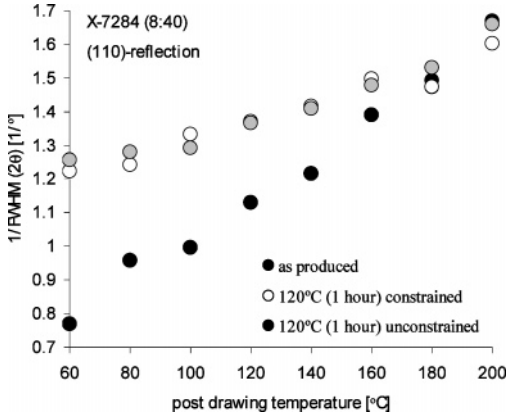

Figure 13. Inverse fwhm of the radial width of the (110) reflection as a function of the initially applied postdrawing temperature.

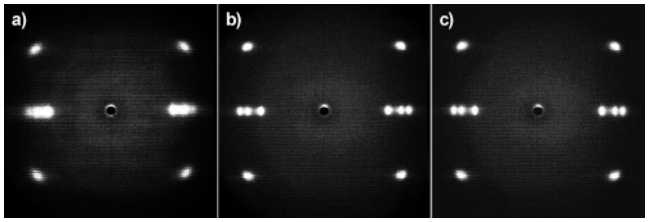

Figure 14. Diffraction patterns of the (X-7284) tape drawn to $\lambda_{PDR} = 5$ at 60 °C: (a) original tape; (b) annealed for 1 h at 120 °C (constrained); (c) annealed for 1 h at 120 °C (unconstrained).

The inverse of the fwhm value of the radial width is shown as a function of the initial postdrawing temperature, indicating the size and/or perfection of the crystals. Again, the data obtained from the initial tapes are included for comparison.

Comparing the data of the initial tapes with the data of annealed samples, it can be seen that the heat treatment improves also the size and/or perfection of the crystals in the (110) direction. The most significant changes are observable for tapes initially postdrawn at low temperatures. Figure 14 shows the diffraction patterns of the tape postdrawn at 60 °C. It is clearly recognizable that the reflections become sharper after heat treatment. Both the arc length and the radial width of the peaks decrease. It is, however, remarkable that the effect of heat treatment is the same for both constrained and unconstrained annealing of the tapes.

For unconstrained tapes, we have determined the dependence of the shrinkage of the postdrawn tapes on postdrawing temperature. In Figure 15, each cross represents an individual measurement, and the open squares represent the average of individual measurements. The measured shrinkage is small for all tapes. In the postdrawing temperature range from 60 to 160 °C the shrinkage varies from 6.4% at 80 °C to 5.4% at 160 °C, followed by a decrease to about 3.7% for the tape postdrawn at 200 °C.

Indications for the Formation of Mesomorphic Phase upon Postdrawing. Solid-state deformation of iPP may result in partial transformation of both amorphous and crystalline phases into the so-called mesomorphic phase. The amount of the induced mesomorphic phase depends on applied deformation temperature and drawing conditions.

Additional DSC and wide-angle X-ray scattering studies were performed to identify the presence of

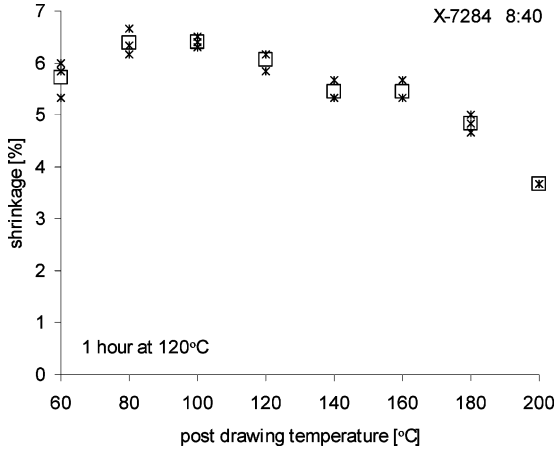

Figure 15. Shrinkage in percentage of the initial sample length as a function of the postdrawing temperature.

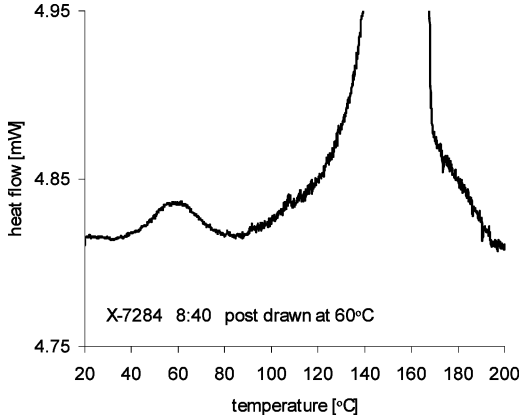

Figure 16. Magnification of the DSC trace of the (X-7284) tape solid-state postdrawn ($\lambda_{PDR} = 5$) at 60 °C.

mesomorphic phase in postdrawn tapes. Figure 16 shows a DSC trace of a X-7284 tape solid state postdrawn at 60 °C to $\lambda_{PDR} = 5$. As reported elsewhere,[8,17,18] the presence of mesomorphic phase is indicated in the DSC trace by a small endothermic peak in the temperature range 40−80 °C (proposed melting of the mesomorphic phase), followed by an exothermic peak (recrystallization into α-crystals), which can, however, be blurred with the onset of the overall melting peak of iPP. In the DSC trace, the endothermic peak at 40−80 °C is clearly visible. However, we did not analyze the dependence of the amount of mesomorphic phase on the applied postdrawing temperature, since it is rather delicate to quantify the area of this small peak.

Another indication for the presence of mesomorphic phase in the sample can be found in the wide-angle X-ray diffraction patterns. Performing integration along the azimuthal angle, the 2-dimensional X-ray patterns are transformed into 1-dimensional plots. As reported by Saraf and Porter,[10] the (110) and (040) peaks shift closer together in the 1-dimensional plot if the mesomorphic phase is present. Figure 18 shows the positions of the maxima of the (110) and (040) peaks of the postdrawn tapes as a function of the postdrawing temperature. In accordance with literature, the decreasing distance between the positions of the maximum of the (110) and the (040) peaks indicates the presence of the mesomorphic phase in, at least, the tapes postdrawn at 60 and 80 °C, respectively.

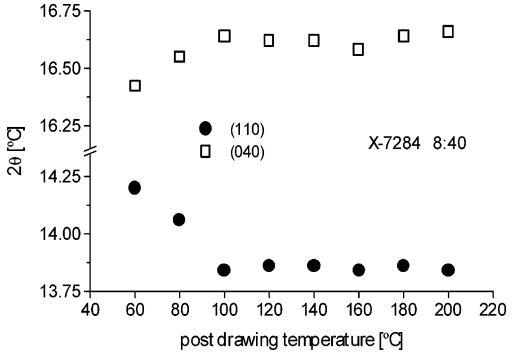

Figure 17. Position of the maxima of the (110) and (040) peaks as a function of the applied postdrawing temperature.

Discussion

In the Results section, it was shown that overall mechanical properties as well as structure and morphology of melt-spun and subsequently solid-state postdrawn iPP tapes (and fibers) depend strongly on the temperature of the postdrawing stage. We now introduce a model to explain the observed structure−processing−property relations.

Before postdrawing in the oven, all tapes possess the same morphology consisting of somewhat oriented lamella crystals embedded in a slightly oriented amorphous matrix. (The predrawing ratio λ_{PRE} induced by the extrusion process was determined to be about 1.6.) Subsequently, the tape is deformed in the oven. For this, stress has to be applied on the tape. In the beginning, the deformation induces mainly stretching of the amorphous phase. At low postdrawing temperatures (below the α-relaxation temperature), the molecular mobility in the crystals is too low for effective relaxation processes on the time scale of the deformation process. This results in an affine deformation. The applied stress can be effectively transferred via the amorphous phase into the crystalline phase, resulting in shearing and final fragmentation of the lamellae into small crystal blocks. The constrained amorphous phase ensures a high orientation of the obtained crystal blocks with respect to the drawing direction. Moreover, the described processing conditions are favorable for the formation of the mesomorphic phase, which can be interpreted as an imperfect crystal structure. The low mobility of the polymer chains at low postdrawing temperatures hinders an effective reorganization to perfect crystals. It can be concluded that at low postdrawing temperatures the morphology consists of small and imperfect crystals kept highly oriented by the constrained amorphous phase.

The high mobility of the polymer chains at elevated postdrawing temperatures allows easy destruction of the crystals and after reorganization their perfection and growth. Even homoepitaxial crystal growing can be observed at high drawing temperatures (180 and 200 °C). However, immediate relaxation of the amorphous phase before complete consolidation of the crystal phase results in a reduced orientation of the crystal phase with respect to the drawing direction.

The described change in morphology explains the observed dependence of mechanical properties on the postdrawing temperature. As mentioned, at low postdrawing temperatures (up to ∼120 °C), the chain mobility in the polymer is too low for effective relaxation processes on the time scale of the deformation process (affine deformation). In accordance with the Irvine−Smith model, the tensile modulus is uniquely determined by the applied postdraw ratio and remains constant (Figure 4). This indicates that the samples have the same average molecular orientation, independent of the postdrawing temperature. At higher drawing temperatures, the chain mobility increases and relaxation processes become more and more dominant during postdrawing. Consequently, a lower molecular orientation is induced upon deformation, resulting in the observed decrease of the tensile modulus.

The described changes in morphology can also explain the dependence of yield stress and elongation at yield on the applied postdrawing temperature. The yield point reflects the onset of crystal deformation upon drawing of the sample. The stress at which deformation of the crystals occurs increases with increasing strength of the intra- and interchain interactions in the crystal. For a particular crystal, the number of interactions (van der Waals bonds) increases with the crystal length in the *c*-direction. The intensity of the interactions depends on the distances between chains in the crystal, which again is affected by the perfection of the crystals in lateral dimensions. Additionally, a high degree and narrow distribution of the crystal orientation are essential to obtain high yield stresses, since this ensures that the individual crystals start to deform simultaneously at a certain extent of elongation.

At low postdrawing temperatures, the deformation process causes a partial transformation of monoclinic α-crystals into mesomorphic phase. The formation of mesomorphic phase facilitates the subsequent deformation of the sample; i.e., the yield stress decreases in a tensile test. Evidence for the formation of mesomorphic phase arises from DSC (Figure 16) as well as X-ray measurements (Figure 17). With increasing postdrawing temperature the amount of mesomorphic phase decreases. Moreover, the enhanced mobility of the polymer chains enables an improvement of existing crystals in both perfection and size. The enhanced coherence in lateral dimension can be seen from the steady increasing 1/fwhm values of the radial width of (110) reflections with increasing postdrawing temperature (Figure 8). TEM images (Figure 10) show the increase of the crystal thickness in the *c*-direction. Moreover, the degree of crystal orientation decreases only slightly with increasing postdrawing temperature up to temperatures of about 160 °C (Figure 11). Consequently, increasing size of the crystals with increasing drawing temperature leads to the observed increase in yield stress (Figure 5).

However, at higher drawing temperatures, chain relaxation during deformation becomes dominant so that the orientation of both amorphous and crystalline phases drops significantly. The decline in orientation of the amorphous phase can be seen from the shrinkage experiment (Figure 15). The amount of shrinkage remains almost constant for tapes postdrawn at temperatures up to 160 °C, while significantly lower shrinkage can be observed for the samples drawn at 180 and 200 °C. The shrinkage results primary from a contraction of the amorphous phase caused by entropic forces, which increase with the extension of the polymer chains. Consequently, the lower shrinkage at 180 and 200 °C suggests that the amorphous phase is already relaxed and consequently less oriented than at lower drawing temperatures.

The decline in orientation of the crystalline phase is reflected by the significant drop in the 1/fwhm values of the arc length of the wide-angle X-ray reflections (Figure 11). Because of broader orientation distribution of the crystals with respect to the drawing direction, the crystals are not deformed simultaneously, since the ease of shear deformation depends on the angle of the crystals with respect to the drawing direction. This leads to the observed drop in yield stress for tapes postdrawn at 180 and 200 °C. The steep increase in elongation at yield results from the low extension of the amorphous phase. Upon drawing the sample in the tensile test, the amorphous phase can be extended before the deformation of the crystals starts.

Finally, the results of annealing experiments (Figures 12−15) are considered. It is rather surprising that the effect of heat treatment is the same in both constrained samples and unconstrained samples. Moreover, the low extent of shrinkage of the unconstrained tapes is also remarkable. These observations suggest that shrinkage of the unconstrained tapes is hindered by the morphology of the postdrawn tapes. A morphology which guarantees such behavior is based on crystals forming a "brick stone" structure. The crystal network keeps the amorphous phase constrained and therefore reduces the overall shrinkage.

The observed increase in both crystal orientation and crystal size and/or perfection results from melting of most imperfect and less oriented crystals and subsequent recrystallization, in which more perfect and higher oriented crystals act as nuclei. Since the annealing temperature is well above the transition temperature, the recrystallization process includes also the transformation of existing mesophase into α-crystals, leading again to a perfection of the crystal structure.

Conclusions

It can be concluded that two different drawing regimes have to be distinguished. In the affine deformation regime, the tensile modulus is independent of the postdrawing temperature used. But the stiffness decreases with increasing postdrawing temperature in the nonaffine deformation regime. In contrast, the drawing temperature strongly affects the overall mechanical behavior of samples in both the affine deformation regime and the nonaffine deformation regime. Lowering the postdrawing temperature within the affine deformation regime results in a drop in yield stress.

The effect of the postdrawing temperature used on the mechanical properties as well as on structure and morphology of solid-state drawn isotactic polypropylene has been described and discussed. For a constant postdraw ratio, samples can be prepared possessing either high stiffness in combination with superior drawability/energy absorption (lowest possible postdrawing temperature, formation of mesomorphic phase) or a high stiffness in combination with high strength (highest postdrawing temperature in the affine deformation regime). The observed dependence of the mechanical behavior of the postdrawn tapes on the drawing temperature used can be explained by changes in their structure and morphology. These changes are displayed by differences in density, crystallinity and/or phase composition, crystal size and/or perfection, and orientation of crystal and amorphous phase. At low postdrawing temperatures, the morphology consists of small and imperfect crystals kept highly oriented by the constrained amorphous phase. DSC and X-ray experiments indicate the presence of the mesomorphic crystal phase of polypropylene. At high postdrawing temperatures, the crystals are large and more perfect but also less oriented with respect to the drawing direction. Moreover, annealing experiments suggest that crystals form a network, which constrains the amorphous phases and reduces its relaxation at elevated temperatures.

Acknowledgment. The authors are thankful to the R&D team from Lankhorst/Indutech B.V. for their help during tape preparation. We acknowledge Novem for financial support of the PURE project, within which the current studies were performed. The authors also thank Frank van de Burgt and Marco Hendrix for their support for X-ray investigation. A special thanks is extended to Ton Peijs, Piet Lemstra, and Cees Bastiaansen for their indefatigable readiness for discussions.

References and Notes

(1) Andreassen, E.; Myhre, O. J.; Hinrichsen, E. L.; Grøstad, K. *J. Appl. Polym. Sci.* **1994**, *52*, 1505.
(2) Irvine, P. A.; Smith, P. *Macromolecules* **1986**, *19*, 240.
(3) Schimanski, T.; Peijs, A. A. J. M.; Lemstra, P. J.; Loos, J. *Macromolecules* **2004**, *37*, 1810.
(4) Sheehan, W. C.; Cole, T. B. *J. Appl. Polym. Sci.* **1964**, *8*, 2359.
(5) Nadella, H. P.; Henson, H. M.; Spruiell, J. E.; White, J. L. *J. Appl. Polym. Sci.* **1977**, *21*, 3003.
(6) Brückner, S.; Meille, S. V.; Petraccone, V.; Pirozzi, B. *Prog. Polym. Sci.* **1997**, *16*, 361.
(7) Auriemma, F.; de Ballesteros, O. R.; de Rosa, C.; Corradini, P. *Macromolecules* **2000**, *33*, 8764.
(8) Fichera, A.; Zannetti, R. *Makromol. Chem.* **1975**, *176*, 1885.
(9) Zannetti, R.; Celotti, G.; Fichera, A.; Francesconi, R. *Makromol. Chem.* **1969**, *128*, 137.
(10) Saraf, R. F.; Porter, R. S. *Polym. Eng. Sci.* **1988**, *28*, 842.
(11) Tung, L. H.; Taylor, W. C. *J. Polym. Sci.* **1956**, *21*, 144.
(12) Kilian, H. G. *Kolloid-Z.* **1961**, *176*, 49.
(13) Nurul, H. M.; Dragaun, H.; Bauer, S.; Muschik, H.; Skalicky, P. *Colloid Polym. Sci.* **1985**, *263*, 730.
(14) Trent, J. S.; Scheinbeim, J. I.; Couchman, P. R. *Macromolecules* **1983**, *16*, 589.
(15) Bakke, J. M.; Bethell, D. *Acta Chem. Scand.* **1992**, *46*, 644.
(16) Satija, S. K.; Wang, C. H. *J. Chem. Phys.* **1978**, *69*, 2739.
(17) Caldas, V.; Brown, G. R.; Nohr, R. S.; MacDonald, J. G.; Raboin, L. E. *Polymer* **1994**, *35*, 899.
(18) Wang, Z.-G.; Hsiao, B. S.; Srinivas, S.; Brown, G. M.; Tsou, A. H.; Cheng, S. Z. D.; Stein, R. S. *Polymer* **2001**, *42*, 7561.

MA051223I